Correlation Renormalized and Induced Spin-Orbit Coupling

Kun Jiang(蒋坤)[1,2*]

[1]*Beijing National Laboratory for Condensed Matter Physics, and Institute of Physics, Chinese Academy of Sciences, Beijing 100190, China*
[2]*School of Physical Sciences, University of Chinese Academy of Sciences, Beijing 100190, China*

(Received 11 November 2022; accepted manuscript online 2 December 2022)

Interplay of spin-orbit coupling (SOC) and electron correlation generates a bunch of emergent quantum phases and transitions, especially topological insulators and topological transitions. We find that electron correlation will induce extra large SOC in multi-orbital systems under atomic SOC and change ground state topological properties. Using the Hartree–Fock mean field theory, phase diagrams of p_x/p_y orbital ionic Hubbard model on honeycomb lattice are well studied. In general, correction of strength of SOC $\delta\lambda \propto (U' - J)$. Due to breaking down of rotation symmetry, form of SOC on multi-orbital materials is also changed under correlation. If a non-interacting system is close to fermionic instability, spontaneous generalized SOC can also be found. Using renormalization group, SOC is leading instability close to quadratic band-crossing point. Mean fields at quadratic band-crossing point are also studied.

DOI: 10.1088/0256-307X/40/1/017102

Successful theoretical proposal of topological insulators triggers intense studies on spin-orbit coupling (SOC) and topological phases.[1,2] In general, SOC is a relativistic effect originated from interactions between the orbital angular momentum $\boldsymbol{L}$ and electron spin $\boldsymbol{S}$ in atoms, which is usually considered as a small perturbation in solids.[3] Atomic SOC is effectively proportional to Z^4, where Z is the atomic number.[4] Thus, insulators from heavily atoms such as Bi and Hg are widely exploited in topological insulator (TI) studies.[1,2] On the other hand, electron-electron correlation strongly varies from more extended orbitals (e.g., s, p) to more localized orbitals (e.g., $3d$, $4d$, $5f$). Strong correlation brings us Mott insulators, magnetism, correlated metallic states and unconventional superconductivity. Noticeably, correlation strengths in correlated systems are much large than SOC and hopping integrals. Bring correlation and SOC together broadly enlarges numbers of emergent quantum phases, from Weyl semimetal, axion insulator to fractional Chern insulator, etc.[4,5] Due to intense study on SOC and correlation, it is natural to ask whether correlation can increase or decrease strength of SOC. Does correlation change the form of SOC? To answer these questions, we construct a Hartree–Fock study on a multi-orbital Hubbard model and show that correlations indeed effect form and strength of SOC. Close to instability, generalized SOC can be spontaneously generated. The great interest in the interplay between correlation and SOC has also been explored in previous works.[6–10]

SOC links orbital Hilbert space with spin Hilbert space by $\boldsymbol{L}\cdot\boldsymbol{S}$. More precisely, $\boldsymbol{L}\cdot\boldsymbol{S} = L_x\otimes S_x + L_y\otimes S_y + L_z\otimes S_z$. Due to crystal field in real materials, we often use real atomic orbital basis like p_x, d_{xz} orbitals rather than eigenbases of L_z, Y_{lm}. Thus, angular momentum $\boldsymbol{L}$ are generally represented by $L_\mu = \sum_{\alpha,\beta} l_{\mu,\alpha,\beta} C^\dagger_\alpha C_\beta$, where $\mu = x, y, z$, α, β are real orbitals, and $l_{\mu,\alpha,\beta}$ are coefficients of L_μ channels. Due to rotation symmetry, all $l_{\mu,\alpha,\beta}$ are related to each other by rotation operators. Since S_z preserves spin and $S_{x/y}$ links up-spin and down-spin, SOC terms contains two types of operators, spin conserving $L_z \otimes S_z$ and spin flipping $L_{x/y} \otimes S_{x/y}$:

$$\begin{aligned} L_z \otimes S_z &= \sum_{\alpha,\beta,\sigma} l_{z,\alpha,\beta} C^\dagger_{\alpha,\sigma} C_{\beta,\sigma}, \\ L_{x/y} \otimes S_{x/y} &= \sum_{\alpha,\beta,\sigma} l_{x/y,\alpha,\beta} C^\dagger_{\alpha,\sigma} C_{\beta,\bar{\sigma}}. \end{aligned} \tag{1}$$

The multi-orbital Hubbard model preserving $O(3)$ rotation symmetry in p, d orbitals[11] reads

$$\begin{aligned} H_U = &\frac{1}{2}U \sum_{i,\alpha,\sigma\neq\sigma'} C^\dagger_{i\alpha\sigma} C^\dagger_{i\alpha\sigma'} C_{i\alpha\sigma'} C_{i\alpha\sigma} \\ &+ \frac{1}{2}U' \sum_{i,\sigma,\sigma',\alpha\neq\beta} C^\dagger_{i\alpha\sigma} C^\dagger_{i\beta\sigma'} C_{i\beta\sigma'} C_{i\alpha\sigma} \\ &+ \frac{1}{2}J \sum_{i,\sigma,\sigma',\alpha\neq\beta} C^\dagger_{i\alpha\sigma} C^\dagger_{i\beta\sigma'} C_{i\alpha\sigma'} C_{i\beta\sigma} \\ &+ \frac{1}{2}J_p \sum_{i,\sigma\neq\sigma',\alpha\neq\beta} C^\dagger_{i\alpha\sigma} C^\dagger_{i\alpha\sigma'} C_{i\beta\sigma'} C_{i\beta\sigma}. \end{aligned} \tag{2}$$

Due to orbital rotation symmetry, $U' = U - 2J$ and $J_p = J$. U/U' terms are intra/inter-orbital direct interactions, respectively. The first J term is Hund's rule exchange interaction, and the second J_p term is the pair hopping interaction. As seen in Eq. (2), U just scatters electrons from the same orbital with different spins, which cannot change or renormalize SOC with orbital flipping operators. To understand relation between correlation and SOC, we need only focus on U' and J.

Perturbatively, only two diagrams contribute self-energy Σ, as shown in Fig. 1(a). Tadpole diagram is typically called the Hartree term while Sunrise diagram is

*Corresponding author. Email: jiangkun@iphy.ac.cn
© 2023 Chinese Physical Society and IOP Publishing Ltd

the Fock term in mean-filed approximation.[12] From the above discussion, there are spin-conserved and spin-flipped SOCs. Spin-conserved channels contain three diagrams in Fig. 1(b). U' gives the Fock term. Hund's J with spin summation gives the Hartree term while pair hopping J without spin sum gives another Hartree diagram. Thus,

$$\delta L_z \otimes S_z \propto (U' - J) G^{\sigma,\sigma}_{\alpha,\beta}(x + 0^+ - x). \tag{3}$$

On the contrary, only Fock diagrams contribute spin-flipped SOC, as shown in Fig. 1(c). We have

$$\delta L_{x/y} \otimes S_{x/y} \propto (U' - J) G^{\sigma,-\sigma}_{\alpha,\beta}(x + 0^+ - x). \tag{4}$$

Here, we only consider self-energy correction to the SOC-correlated system without emergency of spontaneous symmetry breaking orders. If SOC is zero, Green's function parts in Eqs. (3) and (4) are zero, and SOC becomes spontaneous symmetry breaking channels, which can be realized close to instability discussed below. Based on perturbative expansion, correlation renormalizes SOC interactions, and self-energy like corrections are proportional to $(U' - J)$. In all channels, coupling constants are isotropic expect Green's function parts. In previous correlation with SOC works, Hubbard U is the only correlation term and no SOC correction is needed.[4,5] However, in realistic materials, U' and J are not small generally. Hence, SOC must be renormalized and self-consistent calculated. To illustrate and prove this idea, we take the p_x/p_y two-orbital model on honeycomb lattice at half-filling as one example. The p_x- and p_y-orbital physics not only is a theoretical model, but also has been investigated in ultracold-atom optical honeycomb lattice.[13–15] The optical potential around each lattice potential minimum is locally harmonic and a large band gap well separates s- and p-orbital bands. By imposing strong laser beams along z direction, p_z-orbital band can be tuned to high energy levels. In consequence, an ideal p_x- and p_y-orbital system is realized in the artificial honeycomb optical lattice. Furthermore, e_g orbitals on honeycomb lattice can be realized in (111) bilayers of $LaNiO_3$[16] similar to the p_x- and p_y-orbital models.

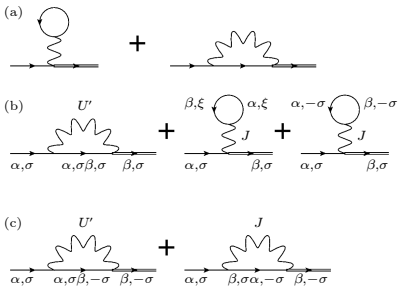

Fig. 1. (a) Hartree diagram and Fock diagram corrections to self-energy Σ. (b) Hartree–Fock corrections to spin conserved SOC $L_z \otimes S_z$. (c) Hartree–Fock corrections to spin flipped SOC $L_{x/y} \otimes S_{x/y}$.

The noninteracting Hamiltonian of the p_x- and p_y-orbital system on honeycomb lattice [Fig. 2(b)] is $H_0 = H_t + H_{\rm SO} + H_V$.[15] SOC part $H_{\rm SO}$ is

$$H_{\rm SO} = -\lambda \sum_i (i p^\dagger_{x,\uparrow} p_{y,\uparrow} - i p^\dagger_{x,\downarrow} p_{y,\downarrow} + \text{H.c.}). \tag{5}$$

Sub-lattice asymmetry or ionic potential V is also added,

$$H_V = V \sum_i (\hat{n}_{i,\rm A} - \hat{n}_{i,\rm B}), \tag{6}$$

where $\hat{n}_{i,\rm A/B}$ are electron density operators for A and B sub-lattices. Clearly, H_0 is electron spin s_z conserved. We introduce the eight-component spinor representation in momentum space defined as

$$p_{\sigma,\tau,\alpha}(k) = (p_{\uparrow,\rm A,x}, p_{\uparrow,\rm A,y}, p_{\uparrow,\rm B,x}, p_{\uparrow,\rm B,y}, \uparrow\to\downarrow), \tag{7}$$

$$H_{t\sigma}(k) = \begin{bmatrix} 0 & T \\ T^+ & 0 \end{bmatrix}, \tag{8}$$

$$T = \begin{bmatrix} t_\pi + \frac{3t_\sigma + t_\pi}{4}(e^{ik_x} + e^{ik_y}) & \frac{\sqrt{3}(t_\sigma - t_\pi)}{4}(e^{ik_x} - e^{ik_y}) \\ \frac{\sqrt{3}(t_\sigma - t_\pi)}{4}(e^{ik_x} - e^{ik_y}) & t_\sigma + \frac{t_\sigma + 3t_\pi}{4}(e^{ik_x} + e^{ik_y}) \end{bmatrix},$$

where k_x and k_y are measured in reciprocal lattice vectors $\vec{b}_{1/2}$ of honeycomb lattice; t_σ and t_π are σ and π bonding strengths. $H_{0\downarrow}$ can be obtained by time reversal symmetry. Throughout this study, we neglect π bonding and t_σ is set to 1. The tight binding bands are shown in Fig. 2(a). There are two exact flat bands when $t_\pi = 0$.

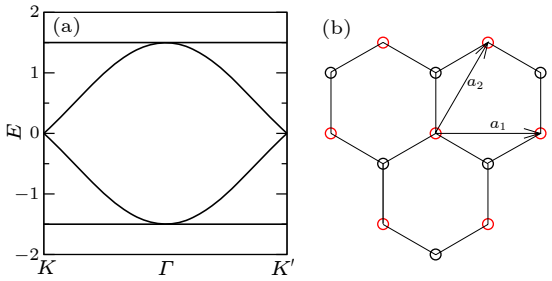

Fig. 2. (a) The electronic band structures for the p_x–p_y model on honeycomb lattice. (b) The crystal structure of honeycomb lattice with translation vectors a_1 and a_2.

Taking all mean field orders equal footing, we decouple H_U to charge $n_{i,\alpha}$, spin $m^\mu_{i,\alpha}$, spin-conserved orbital $L'_{i,\alpha,\beta}$, spin-flip orbital $L''_{i,\alpha,\beta}$, spin-conserved spin-orbital $R'_{i,\alpha,\beta}$, spin-flip spin-orbital $R''_{i,\alpha,\beta}$ channels,[17]

$$\hat{n}_{i,\alpha} = \sum_\sigma \hat{n}^{\alpha\alpha}_{i,\sigma\sigma}, \quad \hat{m}^\mu_{i,\alpha} = \sum_{\sigma\sigma'} \sigma^\mu_{\sigma\sigma'} \hat{n}^{\alpha\alpha}_{i,\sigma\sigma},$$

$$\hat{L'}_{i,\alpha\beta} = \sum_\sigma \hat{n}^{\alpha\beta}_{i,\sigma\sigma} (\alpha \neq \beta), \quad \hat{L''}_{i,\alpha\beta} = \sum_\sigma \hat{n}^{\alpha\beta}_{i,\sigma\bar{\sigma}} (\alpha \neq \beta),$$

$$\hat{R'}_{i,\alpha\beta} = \sum_\sigma \sigma \hat{n}^{\alpha\beta}_{i,\sigma\sigma} (\alpha \neq \beta), \quad \hat{R''}_{i,\alpha\beta} = \sum_\sigma \sigma \hat{n}^{\alpha\beta}_{i,\sigma\bar{\sigma}} (\alpha \neq \beta),$$

$$\hat{n}^{\alpha\beta}_{i,\sigma\sigma'} = C^\dagger_{i,\alpha\sigma} C_{i,\beta\sigma'}. \tag{9}$$

The full mean-field decoupling $H_{\rm MF}$ is listed in the Supplemental Information. Due to emerging charge channels, H_U not only modifies SOC terms and also V terms. In LDA or DFT calculations, tight binding part has already included charge contributions. To avoid double counting, we subtract charge channels.

To simplify the problems, we only focus on $\lambda > 0$ and $V > 0$, and other parameter regions are similar. From perturbation expansions, we find that $\delta\lambda \propto (U' - J)$. The relation between U' and $\delta\lambda$ is shown in Fig. 3(a). At fixed

$\lambda = 0.4$ and $V = 0.5$, $\delta\lambda$ increases monotonically with increasing U', which also enlarges Green function parts. Hence, $\delta\lambda$ is increasing like exponentially. On the contrary, J must disfavor λ. To make sure this point, $\delta\lambda$ is studied in Fig. 3(b) for $U = 0$ and $U' = 0.1J$. Here, we restrict our calculation to $R'_{i,\alpha,\beta}$ only. Large J will induce magnetism m in some parameter regions, which is ignored here. As clearly shown in Fig. 2(b), J decreases $\delta\lambda$, which internally cuts Green's functions. Thus, $\delta\lambda \propto (U' - J)$ is clearly illustrated and correlations change the strength of SOC. Generally, Hubbard U can gain Fock energy from spin $-\frac{2U}{3}\boldsymbol{S}^2$. Just like U, U' gains energy from the Fock energy of spin-orbital $-\frac{U'}{2}|\boldsymbol{L}\cdot\boldsymbol{S}|^2$. However, J can only gain Hartree energy $-J\boldsymbol{S}_{\boldsymbol{\alpha}}\cdot\boldsymbol{S}_{\boldsymbol{\beta}}$ and cost Fock energy from SOC.

The relation between $\delta\lambda$ and λ is plotted in Fig. 3(c). Fixing U' and V, $\delta\lambda$ first increases with increasing λ, and then saturates in the end at $U = J = 0$, $V = 0.5$, $U' = 1$. The saturation is due to fact that Green's function parts of Eqs. (3) and (4) are bounded less than 1. Thus, $\delta\lambda \leq \frac{1}{2}(U' - J) = 0.5$. More interestingly, if staring with trivial insulator, topological nontrivial phases quantum spin Hall (QSH) or TI with spin Chern number $C_s = 1$ can be obtained by tuning U' or λ, as shown in Figs. 3(a) and 3(c). Thus, by turning correlations, different topological phases can be realized in the multi-orbital system.

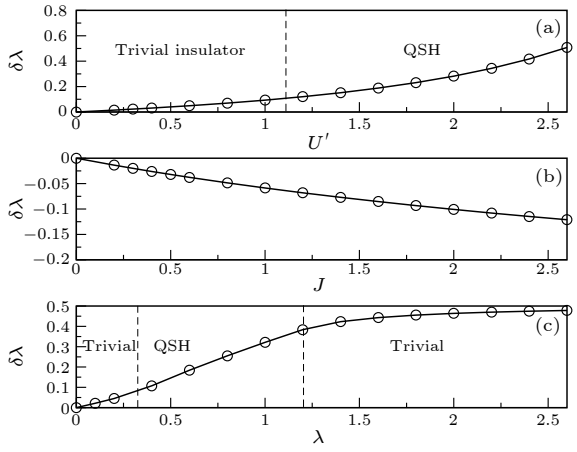

Fig. 3. (a) Behavior of $\delta\lambda$ versus U' at $V = 0.5$, $\lambda = 0.4$, $J = 0.1U'$, $U = 0$, (b) $\delta\lambda$ versus J at $V = 0.5$, $\lambda = 0.4$, $U' = 0.1J$, $U = 0$, (c) $\delta\lambda$ versus λ at $V = 0.5$, $U = 0$, $J = 0$, $U' = 1$.

Single band honeycomb lattice is anti-ferromagnetic in large U.[18] By including all possible channels without doubling counting charge, the phase diagram as functions of U and V is obtained in Fig. 4 at $\lambda = 0.4$ and $J = 0.1U$. When $U = 0$, phase boundary between trivial insulator and QSH is $V = \lambda = 0.4$. Then, slightly increasing U, λ increases and phase boundary is shifted upwards. More precisely, larger $V > 0.4$ is needed for transition from QSH to trivial insulator. Keep enlarging U, magnetism shows up. As found in Ref. [15], if magnetic moments are small, quantum anomalous Hall (QAH) phase ordering in spin z direction is the ground state with the total Chern number $C = 1$ for the whole system. Moreover, if magnetic moments are large, trivial anti-ferromagnetism (T-AFM) ordering in spin xy plane is the ground state. Interestingly, when magnetism $m \neq 0$, orbital order parameter $L_z \neq 0$ induced from finite spin-orbital coupling $L_z \otimes S_z$. Generally, anti-ferromagnetism (AFM) competes with ionic potential V. Thus, if V is smaller, U induces AFM directly from QSH to T-AFM with large magnetic moments while larger V brings magnetic moments down to QAH. However, even larger U always enhances AFM to T-AFM. By tuning U, V and λ, different topological phase transitions can be realized in Fig. 4.

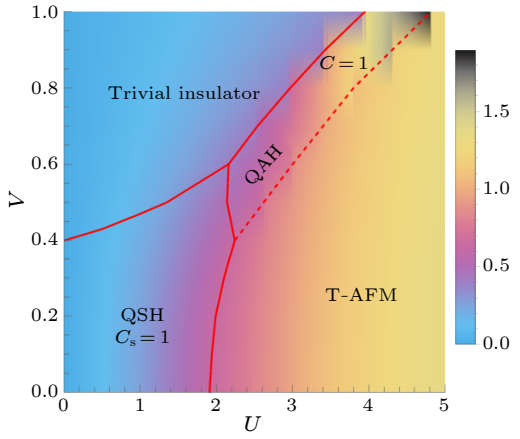

Fig. 4. Phase diagram as functions of U and V with $\lambda = 0.4$. There are four phases, trivial insulator, QSH (quantum spin Hall effect) with spin Chern number $C_s = 1$, QAH (quantum anomalous Hall effect) for Chern number $C = 1$ with spin along z direction, and T-AFM (trivial anti-ferromagnetism) with spin along xy plane. Colors are functions of $\frac{\delta\lambda}{\lambda}$ ratio.

From the above discussion, SOC can be effectively changed from U' and J terms. Thus, in realistic materials, do these change form of SOC? From the definition of SOC, SOC relies on angular momentum $\boldsymbol{L}$, which are generators of space rotation group $SO(3)$. In realistic systems, $SO(3)$ breaks down to point group due to crystal potential. For example, in cuprates, $SO(3)$ is replaced by O_h point group symmetry, where t_{2g} and e_g orbitals are well separated by crystal field. If further including John–Teller distortion, only xz and yz orbitals are degenerate with D_{4h} symmetry. Angular momentum L is not a good defined quantum operator there. The form of new emerged SOC is only protected by space group symmetry. In other words, under $SO(3)$, all $l_{\mu,\alpha,\beta}$ are related to each other by $SO(3) \otimes SU(2)$ rotation about $\hat{\boldsymbol{n}}$ by θ, $R(\hat{\boldsymbol{n}},\theta) = \exp(i\boldsymbol{L}\cdot\hat{\boldsymbol{n}}\theta) \otimes \exp(i\boldsymbol{S}\cdot\hat{\boldsymbol{n}}\theta)$. However, under space group $\otimes SU(2)$, only a few $l_{\mu,\alpha,\beta}$ are related. SOC $\boldsymbol{L}\cdot\boldsymbol{S}$ should change to $\boldsymbol{L}_{\boldsymbol{\alpha},\boldsymbol{\beta}}\cdot\boldsymbol{S}$ due to breaking down of $SO(3)$ rotation symmetry. Hence, generally SOC should be replaced by

$$\lambda\langle\alpha|\boldsymbol{L}|\beta\rangle\langle\sigma|\boldsymbol{S}|\sigma'\rangle \to \lambda_{\alpha,\beta}\langle\alpha|\boldsymbol{L}|\beta\rangle\langle\sigma|\boldsymbol{S}|\sigma'\rangle. \tag{10}$$

Interestingly, the SOC-type terms can also be generated dynamically or spontaneously close to instabilities from correlation.[16,19] Thus, it is also natural to ask whether multi-orbital systems can generate SOC spontaneously. For $\lambda = 0$ and arbitrary V, H_0 at Γ point has two quadratic band-crossing points (QBCPs) with $t_\sigma = 1$

and $t_\pi = -0.2$, as shown in Figs. 5(a) ($V = 0$) and 5(c) ($V = 0.3$). QBCPs are marginally unstable to arbitrarily weak repulsive interactions.[20–22] By the quarter-filling p_x–p_y model, QBCPs are achieved with a nearly flat band. We can expand the models around QBCPs, and find out the leading instability from renormalization group. After careful calculations,[17] renormalization group beta equations can be written as

$$\begin{aligned}
\frac{-\partial U}{\partial l} &= [2U'^2 - J^2 + 2U(-2U' + J + J_p)]\gamma \\
&\quad + (UJ + UU' - U'J)\gamma + (U^2 + J_p^2)\eta, \\
\frac{-\partial U'}{\partial l} &= [-U'^2 - U^2 + J^2 + 2U'(2U + J + J_p)]\gamma \\
&\quad - (UJ - U'J + U'U)\gamma - (U'^2 + J_p^2)\eta, \\
\frac{-\partial J}{\partial l} &= [2J^2 + U^2 + U'^2 + 2J(-U + U' - 2J_p)]\gamma \\
&\quad + J_P(U' + J)\gamma + (2J^2 + J_p^2 - U'J)\eta, \\
\frac{-\partial J_p}{\partial l} &= (U^2 + U'^2 - 2J^2 + JU' + J_P^2)\gamma \\
&\quad + J_p(2U - 3U' + 3J)\eta. \qquad (11)
\end{aligned}$$

Here, γ and η are integrals related to one-loop diagrams and functions of t_π and t_σ, which can be calculated numerically.[22] To QBCPs, η is always large than γ. Flows of interactions are shown in Fig. 5(a). U' and J_p diverge quickly to $\pm\infty$, respectively. U and J flow as U' and J divergence.

We have the interaction vertex coupling to order parameters as follows:

$$\begin{aligned}
&L_z\boldsymbol{S} \to g_1 = (U' - J_p)\eta, \\
&L_z \to g_2 = (U' + J_p - 2J)\eta, \\
&\tau_x \to g_3 = (U' - 2J - J_p)(\eta - 2\gamma), \\
&\tau_x\boldsymbol{S} \to g_4 = (U' + J_p)(\eta - 2\gamma), \\
&\tau_z \to g_5 = (-U + 2U' - J)2\gamma, \\
&\tau_z\boldsymbol{S} \to g_6 = (U - J)2\gamma. \qquad (12)
\end{aligned}$$

Interaction vertex coupling directly to spin $\boldsymbol{S}$ is zero. Three leading instabilities are g_1, g_3, g_5. Here, g_1 for SOC $L_z\boldsymbol{S}$ is leading instability; g_3 corresponds to orbital polarization, and g_5 is ferro-orbital order. These RG results agree with conclusions of Refs. [20,21]. As described in Ref. [20], g_1 can gap out the QBCPs while $g_{3/5}$ only shift the QBCPs to two Dirac points.

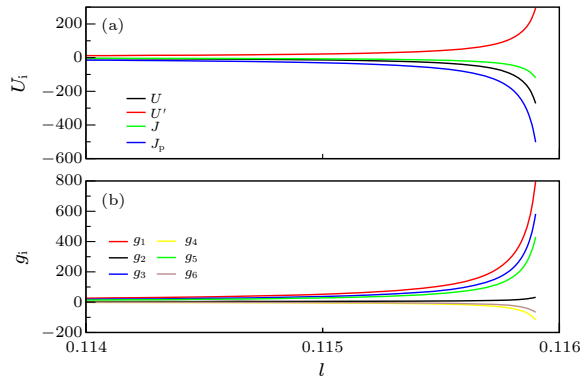

Fig. 5. (a) RG flows of U, U', J, J_p. (b) RG flows of g_i, dominated by g_1 ($\tau_y S$ SOC), g_3 (τ_x orbital polarization), g_5 (τ_z ferro-orbital order).

After self-consistent calculations, we also find that $L_z \otimes \boldsymbol{S}$ are leading orders, whose bands are shown in Figs. 6(b) and 6(d). $L_z \otimes \boldsymbol{S}$ means that the system can order in any spin direction like $L_z \otimes S_{x/y}$, which are not included in atomic SOC $L_z \otimes S_z$. Noninteracting p_x- and p_y-orbital model remains spin $SU(2)$ symmetry and can spontaneously break down to $U(1)$ with generalized spin orbital $L_z \otimes \boldsymbol{S}$. If $V = 0$, bands remain spin degenerate, as shown in Fig. 5(b). However, when V is finite, inversion symmetry is breaking and spin degeneration is split except at the Γ point, as shown in Fig. 6(d). Noticeably, time reversal still protects $E(k,\uparrow) = E(-k,\downarrow)$. Also, just as in the renormalized SOC case, J does not help generating such a kind of order.

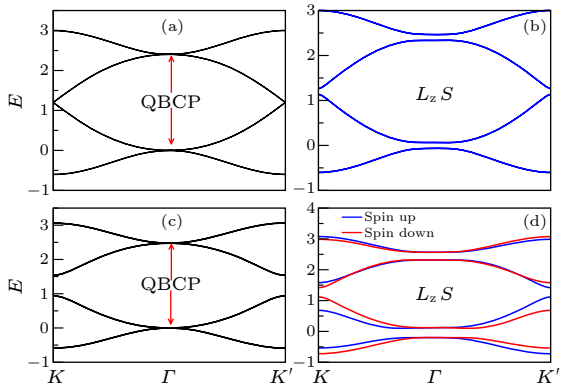

Fig. 6. (a) Bands of H_0 with $\lambda = 0$, $V = 0$, $t_\sigma = 1$, $t_\pi = -0.2$ and two QBCPs around the Γ point. (b) Bands of $L_z \otimes \boldsymbol{S}$ order with $\lambda = 0$, $V = 0$, $U = 1.6$, $J = 0$. Blue lines are bands for up-spin while red lines for down-spin in $L_z \otimes S_z$ order. (c) Bands of H_0 with $\lambda = 0$, $V = 0.3$, $t_\sigma = 1$, $t_\pi = -0.2$ and two QBCPs around the Γ point. (d) Bands of $L_z \otimes \boldsymbol{S}$ order with $\lambda = 0$, $V = 0.3$, $U = 1.6$, $J = 0$.

For general $\boldsymbol{L}$ and $\boldsymbol{S}$ combination, we can have one scalar (one-dimensional) $\boldsymbol{L} \cdot \boldsymbol{S}$, one vector (three-dimensional) $\boldsymbol{L} \times \boldsymbol{S}$ and one quadrupole operator (five-dimensional) $Q_{\mu\nu} = \frac{1}{2}(L_\mu S_\nu + L_\nu S_\mu) - \frac{1}{3}\boldsymbol{L} \cdot \boldsymbol{S}$. Thus, with correlation and instability, the system can generate any above combinations of $\boldsymbol{L}$ and $\boldsymbol{S}$, including $L_z \otimes S_y$ order we found. Further breaking rotation symmetry, more spin orbital coupling terms, like $\boldsymbol{L} \cdot \boldsymbol{S} \to \boldsymbol{L}_{\boldsymbol{\alpha},\boldsymbol{\beta}} \cdot \boldsymbol{S}$, are available for further discussion.

In summary, multi-orbital correlation could induce large renormalization of SOC proportional to $U' - J$. In realistic materials, due to lowering symmetry of space group compared to $SO(3)$, the form of SOC is also changed according to Eq. (10) $\boldsymbol{L} \cdot \boldsymbol{S} \to \boldsymbol{L}_{\boldsymbol{\alpha},\boldsymbol{\beta}} \cdot \boldsymbol{S}$. Thus, SOC correction from $U' - J$ should be considered consistently. In previous works, relations between correlation and SOC have also been discussed, which are consistent with our conclusions.[6–10,23,24] Experimentally, orbital-dependent SOC may be the origin of orbital-dependent splitting band gap observed in angle resolved photoemission spectroscopy.[25,26] More than that, correlated induced SOC may enhance topological non-trivial effect and spin-orbital coupled Mott insulator in d-orbital systems, like iridates.[27–29] Close to instabilities, more generalized SOC terms can be generated spontaneously. It is hope-

ful that these findings will further stimulate the search for enhanced orbital-dependent SOC and correlation induced quantum phases.

Note that, when finalizing this work, we became aware of another work working on correlated spin-orbit coupling with similar results.[30]

Acknowledgments. This work was supported by the National Natural Science Foundation of China (Grant Nos. 11888101 and 12174428), and the Strategic Priority Research Program of Chinese Academy of Sciences (Grant No. XDB28000000).

References

[1] Hasan M Z and Kane C L 2010 *Rev. Mod. Phys.* **82** 3045
[2] Qi X L and Zhang S C 2011 *Rev. Mod. Phys.* **83** 1057
[3] Ashcroft N W and Mermin N D 1972 *Solid State Physics* (New York: Rinehart and Winston)
[4] Witczak-Krempa W, Chen G, Kim Y B, and Balents L 2014 *Annu. Rev. Condens. Matter Phys.* **5** 57
[5] Balents D P A L 2010 *Nat. Phys.* **6** 376
[6] Liu G Q, Antonov V N, Jepsen O, and Andersen O K 2008 *Phys. Rev. Lett.* **101** 026408
[7] Zhang G R, Gorelov E, Sarvestani E, and Pavarini E 2016 *Phys. Rev. Lett.* **116** 106402
[8] Kim M, Mravlje J, Ferrero M, Parcollet O, and Georges A 2018 *Phys. Rev. Lett.* **120** 126401
[9] Li J, Yao Q, Wu L, Hu Z, Gao B, Wan X, and Liu Q 2022 *Nat. Commun.* **13** 919
[10] Qiu W X, Zou J Y, Luo A Y, Cui Z H, Song Z D, Gao J H, Wang Y L, and Xu G 2021 *Phys. Rev. Lett.* **127** 147202
[11] Coury M E A, Dudarev S L, Foulkes W M C, Horsfield A P, Ma P W, Spencer J S 2016 *Phys. Rev. B* **93** 075101
[12] Fetter A and Walecka J 2003 *Quantum Theory of Many-Particle Systems* (New York: Dover)
[13] Wu C J, Bergman D, Balents L, and Sarma S D 2007 *Phys. Rev. Lett.* **99** 070401
[14] Wu C J 2008 *Phys. Rev. Lett.* **100** 200406
[15] Zhang G F, Li Y, and Wu C 2014 *Phys. Rev. B* **90** 075114
[16] Yang K Y, Zhu W, Di X, Okamoto S, Wang Z, and Ran Y 2011 *Phys. Rev. B* **84** 201104(R)
[17] See the Supplemental Material for more detailed discussions.
[18] Zhou S, Wang Y, and Wang Z 2014 *Phys. Rev. B* **89** 195119
[19] Wu C J and Zhang S C 2004 *Phys. Rev. Lett.* **93** 036403
[20] Sun K, Yao H, Fradkin E, and Kivelson S A 2009 *Phys. Rev. Lett.* **103** 046811
[21] Murray J M and Vafek O 2014 *Phys. Rev. B* **89** 201110(R)
[22] Tsai W F, Fang C, Yao H, and Hu J P 2015 *New J. Phys.* **17** 055016
[23] Liechtenstein A I, Anisimov V I, and Zaanen J 1995 *Phys. Rev. B* **52** R5467(R)
[24] Dudarev S L, Botton G A, Savrasov S Y, Humphreys C J, and Sutton A P 1998 *Phys. Rev. B* **57** 1505
[25] Zhang P, Qian T, Richard P, Wang X P, Miao H, Lv B Q, Fu B B, Wolf T, Meingast C, Wu X X, Wang Z Q, Hu J P, and Ding H 2015 *Phys. Rev. B* **91** 214503
[26] Suzuki Y, Shimojima T, Sonobe T, Nakamura A, Sakano M, Tsuji H, Omachi J, Yoshioka K, Kuwata-Gonokami M, Watashige T, Kobayashi R, Kasahara S, Shibauchi T, Matsuda Y, Yamakawa Y, Kontani H, and Ishizaka K 2015 *Phys. Rev. B* **92** 205117
[27] Jackeli G and Khaliullin G 2009 *Phys. Rev. Lett.* **102** 017205
[28] Wang F and Senthil T 2011 *Phys. Rev. Lett.* **106** 136402
[29] Zhou S, Jiang K, Chen H, and Wang Z 2017 *Phys. Rev. X* **7** 041018
[30] Kubo K 2022 *J. Phys. Soc. Jpn.* **91** 124707

Supplemental Material: Correlation renormalized and induced spin-orbit coupling

Kun Jiang*
Beijing National Laboratory for Condensed Matter Physics and Institute of Physics, Chinese Academy of Sciences, Beijing 100190, China and
School of Physical Sciences, University of Chinese Academy of Sciences, Beijing 100190, China
(Dated: December 9, 2022)

PACS numbers:

In this supplemental material, we provide the details of the Hartree-Fock mean field of multi-orbital Hubbard model H_U. Following six channels are decoupled

$$\begin{aligned}
\hat{n}_{i,\alpha} &= \sum_{\sigma} \hat{n}^{\alpha\alpha}_{i,\sigma\sigma} \\
\hat{m}^{\mu}_{i,\alpha} &= \sum_{\sigma\sigma'} \sigma^{\mu}_{\sigma\sigma'} \hat{n}^{\alpha\alpha}_{i,\sigma\sigma} \\
\hat{L'}_{i,\alpha\beta} &= \sum_{\sigma} \hat{n}^{\alpha\beta}_{i,\sigma\sigma} (\alpha \neq \beta) \\
\hat{L''}_{i,\alpha\beta} &= \sum_{\sigma} \hat{n}^{\alpha\beta}_{i,\sigma\bar{\sigma}} (\alpha \neq \beta) \\
\hat{R'}_{i,\alpha\beta} &= \sum_{\sigma} \sigma \hat{n}^{\alpha\beta}_{i,\sigma\sigma} (\alpha \neq \beta) \\
\hat{R''}_{i,\alpha\beta} &= \sum_{\sigma} \sigma \hat{n}^{\alpha\beta}_{i,\sigma\bar{\sigma}} (\alpha \neq \beta) \\
\hat{n}^{\alpha\beta}_{i,\sigma\sigma'} &= C^{\dagger}_{i,\alpha\sigma} C_{i,\beta\sigma'}
\end{aligned} \tag{1}$$

Then, H_U is decoupled as

$$\begin{aligned}
H_U &= \sum_{i,\alpha} [\frac{U}{2} n_{i,\alpha} + (U' - \frac{J}{2}) \sum_{\alpha\neq\beta} n_{i,\beta}] \hat{n}_{i,\alpha} \\
&- \sum_{i,\alpha\mu} [\frac{U}{2} m^{\mu}_{i,\alpha} + \frac{J}{2} \sum_{\alpha\neq\beta} m^{\mu}_{i,\beta}] \hat{m}^{\mu}_{i,\alpha} \\
&+ \sum_{i,\alpha\neq\beta} [(-\frac{U'}{2} + J) L'_{i,\beta\alpha} + \frac{J}{2} L'_{i,\alpha\beta}] \hat{L'}_{i,\alpha\beta} \\
&- \sum_{i,\alpha\neq\beta} [\frac{U'}{2} L''_{i,\beta\alpha} + \frac{J}{2} L''_{i,\alpha\beta}] \hat{L''}_{i,\alpha\beta} \\
&- \sum_{i,\alpha\neq\beta} [\frac{U'}{2} R'_{i,\beta\alpha} + \frac{J}{2} R'_{i,\alpha\beta}] \hat{R'}_{i,\alpha\beta} \\
&+ \sum_{i,\alpha\neq\beta} [\frac{U'}{2} R''_{i,\beta\alpha} + \frac{J}{2} R''_{i,\alpha\beta}] \hat{R''}_{i,\alpha\beta} + const.
\end{aligned} \tag{2}$$

To understand general mean-field orders, for N general orbits, all the general orbital orders are represent as $N*N$ Hermitian matrices.

$$< O_{\alpha\beta} > = < \eta C^{\dagger}_{\alpha} C_{\beta} + \eta^{*} C^{\dagger}_{\beta} C_{\alpha} > \tag{3}$$

where η is coefficient.

$N * N$ Hermitian matrices can be decomposed using SU(N) generators and identity matrix. SU(N) Lie algebra contains $N^2 - 1$ generators, or named orbital isospin operators. We always choose three types of matrices as extension Pauli matrices in SU(2). In defining representation, symmetric non-diagonal σ_x is extended to $T^{(1)}_{\alpha\beta}$ and its matrix as

$$(T^{(1)}_{\alpha\beta})_{ab} = \frac{1}{2} (\delta_{\alpha a}\delta_{\beta b} + \delta_{\beta a}\delta_{\alpha b}) \ (\alpha < \beta) \tag{4}$$

where α/β are labels for generators and a, b are matrices indices. All of them are ranging 1 to N.

And anti-symmetry σ_y is extended as $T^{(2)}_{\alpha\beta}$

$$(T^{(2)}_{\alpha\beta})_{ab} = \frac{-i}{2} (\delta_{\alpha a}\delta_{\beta b} - \delta_{\beta a}\delta_{\alpha b}) \ (\alpha < \beta) \tag{5}$$

The third traceless diagonal σ_z is extended as $T^{(3)}_{\alpha}(\alpha > 1)$ and normalized as

$$(T^{(3)}_{\alpha})_{ab} = \begin{cases} \delta_{ab}(2\alpha(\alpha-1))^{-1/2}, & \text{if } a < \alpha, \\ -\delta_{ab}(\frac{(\alpha-1)}{2\alpha})^{-1/2}, & \text{if } a = \alpha, \\ 0, & \text{if } a > \alpha \end{cases} \tag{6}$$

We have $\frac{N(N-1)}{2}$ symmetric $T^{(1)}_{\alpha\beta}$, anti-symmetric $\frac{N(N-1)}{2}$ $T^{(2)}_{\alpha\beta}$ and traceless $N-1$ $T^{(3)}_{\alpha}$ with total number of generators $N^2 - 1$. Including identity labeled T^3_1, we have full N^2 basis for $N * N$ matrices.

Taking $SU(3)$ for example, $T^{(1)}_{\alpha\beta}$ are

$$T^{(1)}_{12} = \frac{\lambda_1}{2} = \frac{1}{2} \begin{bmatrix} 0 & 1 & 0 \\ 1 & 0 & 0 \\ 0 & 0 & 0 \end{bmatrix} \tag{7}$$

$$T^{(1)}_{13} = \frac{\lambda_4}{2} = \frac{1}{2} \begin{bmatrix} 0 & 0 & 1 \\ 0 & 0 & 0 \\ 1 & 0 & 0 \end{bmatrix} \tag{8}$$

$$T^{(1)}_{23} = \frac{\lambda_6}{2} = \frac{1}{2} \begin{bmatrix} 0 & 0 & 0 \\ 0 & 0 & 1 \\ 0 & 1 & 0 \end{bmatrix} \tag{9}$$

$T^{(2)}_{\alpha\beta}$ are

$$T^{(2)}_{12} = \frac{\lambda_2}{2} = \frac{1}{2}\begin{bmatrix} 0 & -i & 0 \\ i & 0 & 0 \\ 0 & 0 & 0 \end{bmatrix} \quad (10)$$

$$T^{(2)}_{13} = \frac{\lambda_5}{2} = \frac{1}{2}\begin{bmatrix} 0 & 0 & -i \\ 0 & 0 & 0 \\ i & 0 & 0 \end{bmatrix} \quad (11)$$

$$T^{(2)}_{23} = \frac{\lambda_7}{2} = \frac{1}{2}\begin{bmatrix} 0 & 0 & 0 \\ 0 & 0 & -i \\ 0 & i & 0 \end{bmatrix} \quad (12)$$

$T^{(3)}_{\alpha}$ are

$$T^{(3)}_{2} = \frac{\lambda_3}{2} = \frac{1}{2}\begin{bmatrix} 1 & 0 & 0 \\ 0 & -1 & 0 \\ 0 & 0 & 0 \end{bmatrix} \quad (13)$$

$$T^{(3)}_{3} = \frac{\lambda_8}{2} = \frac{1}{2\sqrt{3}}\begin{bmatrix} 1 & 0 & 0 \\ 0 & 1 & 0 \\ 0 & 0 & -2 \end{bmatrix} \quad (14)$$

where λ_i are well-known Gell-Mann matrices for $SU(3)$.

For diagonal orders, identity $T^{(3)}_1$ is total density. And other $T^{(3)}_{\alpha}$ are ferro-orbital orders and crystal field for α and β orbits. Typically, crystal field is diagonal and ferro-orbital for different crystal field class. For example, t_{2g} are more occupied than e_g orbitals in octahedral environment.

For symmetric $T^{(1)}_{\alpha\beta}$, orders are represent as

$$< T^{(1)}_{\alpha\beta} >= \frac{1}{2} < C^{\dagger}_{\alpha} C_{\beta} + C^{\dagger}_{\beta} C_{\alpha} > \quad (15)$$

$T^{(1)}_{\alpha\beta}$ are off-diagonal density matrix for correlated orbitals defined in LDA+U, which are also named on-site interorbial single-electron hopping.

For ani-symmetric $T^{(2)}_{\alpha\beta}$, orders are represent as

$$< T^{(2)}_{\alpha\beta} >= \frac{i}{2} < C^{\dagger}_{\alpha} C_{\beta} - C^{\dagger}_{\beta} C_{\alpha} > \quad (16)$$

Using real orbits, orbital angular momentum L_i are always complex and anti-symmetry as in $T^{(2)}_{\alpha\beta}$. Angular momentums L_i are well defined in SO(3) symmetric systems. For general lattices, L_i are not defined. Thus, we extend 3 L_i in 3D to generalized $\frac{N(N-1)}{2}$ orbital angular momentum $T^{(2)}_{\alpha\beta}$. For $N > 3$, there are more than 3 angular momentums. Angular momentums are expanded as

$$L_i = \sum_{\alpha\beta} l^i_{\alpha\beta} T^{(2)}_{\alpha\beta} \quad (17)$$

$l^i_{\alpha\beta}$ are coefficients of L_i.

In general, local Fermionic Hilbert space is spanned by orbital and spin tensor space. Spin order is defined as Pauli matrices σ_i in SU(2). For charge order including ferro-orbital orders, with number N-1 (1 for total charge)

$$\hat{n}_{\alpha} = \sum_{\beta} n_{\alpha\beta} T^{(3)}_{\beta} \otimes \sigma_0 \quad (18)$$

For general spin order, with number 3N

$$\hat{m}^{\mu}_{\alpha} = \sum_{\beta} m_{\alpha\beta} T^{(3)}_{\beta} \otimes \sigma_{\mu} \quad (19)$$

Then we have general symmetric orbital orders, with number $\frac{N(N-1)}{2}$

$$\hat{O}_{\alpha\beta} = T^{(1)}_{\alpha\beta} \otimes \sigma_0 \quad (20)$$

Generalized anti-symmetric angular momentum orders, with number $\frac{N(N-1)}{2}$

$$\hat{L}_{\alpha\beta} = T^{(2)}_{\alpha\beta} \otimes \sigma_0 \quad (21)$$

Orbital order with spin order, with number $\frac{3N(N-1)}{2}$

$$\hat{OS}^{\mu}_{\alpha\beta} = T^{(1)}_{\alpha\beta} \otimes \sigma_{\mu} \quad (22)$$

Generalized spin-orbital coupling, with number $\frac{3N(N-1)}{2}$

$$\hat{LS}^{\mu}_{\alpha\beta} = T^{(2)}_{\alpha\beta} \otimes \sigma_{\mu} \quad (23)$$

The relations between order defined here and $\hat{L}'$,$\hat{L}''$, $\hat{R}'$,$\hat{R}''$.

$$Re(\hat{L'}_{\alpha\beta}) = \hat{O}_{\alpha\beta} \propto U' - 3J \quad (24)$$

$$Im(\hat{L'}_{\alpha\beta}) = \hat{L}_{\alpha\beta} \propto U' - J \quad (25)$$

$$Re(\hat{R'}_{\alpha\beta}) = \hat{OS}^{z}_{\alpha\beta} \propto U' + J \quad (26)$$

$$Im(\hat{R'}_{\alpha\beta}) = \hat{LS}^{z}_{\alpha\beta} \propto U' - J \quad (27)$$

$$Re(\hat{L''}_{\alpha\beta}) = \hat{OS}^{x}_{\alpha\beta} \propto U' + J \quad (28)$$

$$Im(\hat{L''}_{\alpha\beta}) = \hat{LS}^{x}_{\alpha\beta} \propto U' - J \quad (29)$$

$$Re(\hat{R''}_{\alpha\beta}) = \hat{LS}^{y}_{\alpha\beta} \propto U' + J \quad (30)$$

$$Im(\hat{R''}_{\alpha\beta}) = \hat{OS}^{y}_{\alpha\beta} \propto U' - J \quad (31)$$

Re and Im are real and imaginary parts.

The total number of orders for $2N \times 2N$ matrix are

$$N - 1 + 3N + N(N-1) + 3N(N-1) = 4N^2 - 1 \quad (32)$$

RG part

To to RG, we first need expand around the QBCP with effective continuous model. To keep QBCP, $t_{\pi} < 0$. When $t_{\pi} = 0$, there are two exact flat bands. And when $t_{\pi} > 0$, there are no QBCP anymore without any instability. The low energy effective model is described

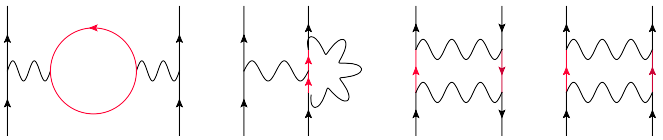

FIG. 1: Four types of one-loop Feynman diagram included in our RG calculations. The red lines are loops integrated.

by $\psi_{p_{x/y},\sigma} = \frac{1}{\sqrt{2}}(\psi_{\sigma,A,p_{x/y}} + \psi_{\sigma,B,p_{x/y}})$. Under this basis transformation, interaction vertices remain same form as in multi-orbital hubbard model.

$$\begin{aligned} H_{QBC}(k) &= \frac{t_\sigma + t_\pi}{2}k^2\sigma_0 + \frac{t_\sigma - t_\pi}{4}(k^2\sigma_z + \sqrt{3}(k_x^2 - k_y^2)\sigma_x) \\ &= d_0\sigma_0 + d_x\sigma_x + d_z\sigma_z \end{aligned} \tag{33}$$

The non-interacting Green's function $(G_0^\sigma(\omega, \mathbf{k}))^{-1} = (i\omega - d_0)\sigma_0 - d_x\sigma_x - d_z\sigma_z$. Then, we integrate out fast modes between cutoff Λ and $\frac{\Lambda}{s}$.We have four interaction vertices and perform one-loop RG including four types of Feynman diagrams. The essentail fermion loop integrals are listed below:

$$ZS1 \ : \ \int_k G^\sigma_{0aa}(k)G^{\sigma'}_{0\bar{a}\bar{a}}(k) = -\eta dl \tag{34}$$

$$ZS2 \ : \ \int_k G^\sigma_{0a\bar{a}}(k)G^{\sigma}_{0\bar{a}a}(k) = \gamma dl \tag{35}$$

$$ZS3 \ : \ \int_k G^\sigma_{0aa}(k)G^{\sigma'}_{0aa}(k) = -\gamma dl \tag{36}$$

$$BCS1 \ : \ \int_k G^\sigma_{0aa}(k)G^{\sigma'}_{0\bar{a}\bar{a}}(-k) = \gamma dl \tag{37}$$

$$BCS2 \ : \ \int_k G^\sigma_{0a\bar{a}}(k)G^{\sigma'}_{0\bar{a}a}(-k) = \gamma dl \tag{38}$$

$$BCS3 \ : \ \int_k G^\sigma_{0aa}(k)G^{-\sigma'}_{0aa}(-k) = \eta dl \tag{39}$$

where $\int_k = \int_{-\infty}^{\infty}\frac{d\omega}{2\pi}\int_0^{2\pi}\frac{d\theta}{2\pi}\int_{\frac{\Lambda}{s}}^{\Lambda}\frac{dk}{2\pi}$ and $s = e^{dl}$. To more precisely,

$$\eta = \int_0^{2\pi} d\theta \frac{f_x^2(\theta) + 2f_z^2(\theta)}{4(f_x^2(\theta) + f_z^2(\theta))^{\frac{3}{2}}} \tag{40}$$

$$\gamma = \int_0^{2\pi} d\theta \frac{f_x^2(\theta)}{4(f_x^2(\theta) + f_z^2(\theta))^{\frac{3}{2}}} \tag{41}$$

$$f_x(\theta) = \frac{\sqrt{3}}{4}(t_\sigma - t_\pi)(\cos\theta^2 - \sin\theta^2) \tag{42}$$

$$f_z(\theta) = \frac{1}{4}(t_\sigma - t_\pi)(\cos\theta^2 + \sin\theta^2) \tag{43}$$

In Figs.2-5, we list all one-loop Feynman diagrams contributing to interaction renormalization.

* Electronic address: jiangkun@iphy.ac.cn

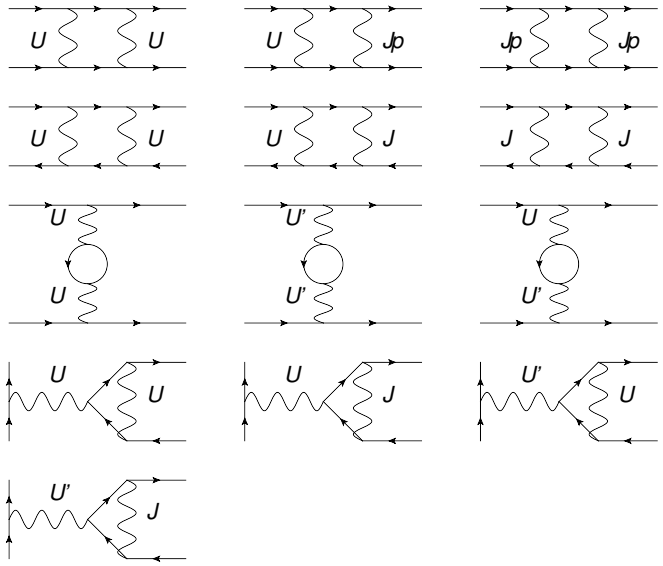

FIG. 2: Feynman diagrams contributing to U renormalization.

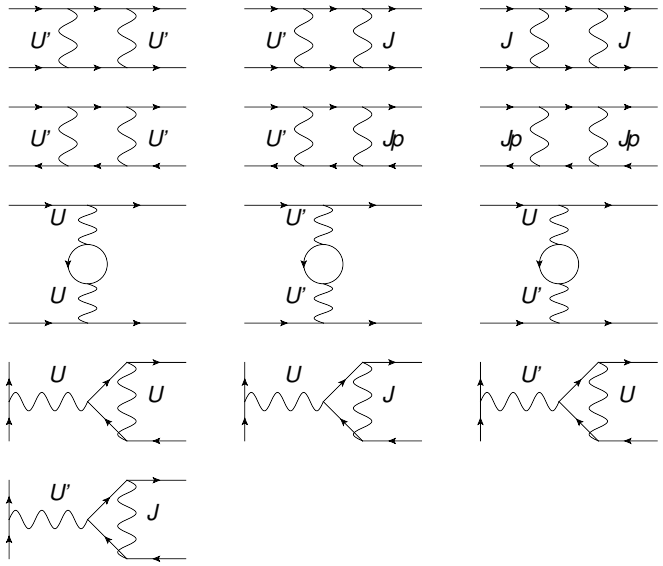

FIG. 3: Feynman diagrams contributing to U' renormalization.

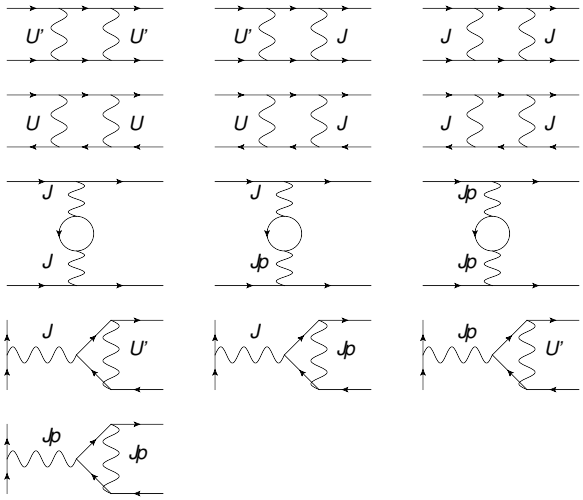

FIG. 4: Feynman diagrams contributing to J renormalization.

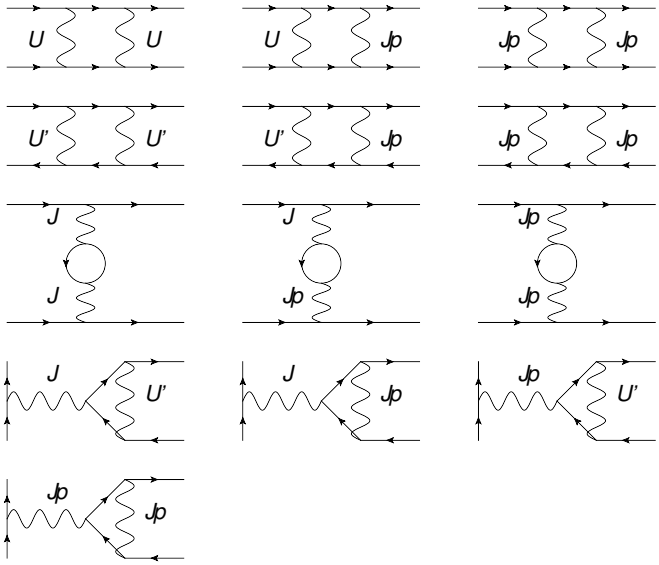

FIG. 5: Feynman diagrams contributing to J_p renormalization.